Carbohydrate Polymers 237 (2020) 116162

Contents lists available at ScienceDirect

Carbohydrate Polymers

journal homepage: www.elsevier.com/locate/carbpol

Effect of electrical discharge plasma on cytotoxicity against cancer cells of *N,O*-carboxymethyl chitosan-stabilized gold nanoparticles

Chayanaphat Chokradjaroen[a], Ratana Rujiravanit[a,b,*], Sewan Theeramunkong[c], Nagahiro Saito[d]

[a] The Petroleum and Petrochemical College, Chulalongkorn University, Bangkok, 10330, Thailand
[b] Center of Excellence on Petrochemical and Materials Technology, Chulalongkorn University, Bangkok, 10330, Thailand
[c] Faculty of Pharmacy, Thammasat University, Pathumthani, 12120, Thailand
[d] Department of Chemical Systems Engineering, Graduate School of Engineering, Nagoya University, Nagoya, 464-8603, Japan

ARTICLE INFO

Keywords:
Gold nanoparticles
N,O-carboxymethyl chitosan
Cytotoxicity
Cancer cells
Electrical discharge plasma

ABSTRACT

Electrical discharge plasma in a liquid phase can generate reactive species, *e.g.* hydroxyl radical, leading to rapid reactions including degradation of biopolymers. In this study, the effect of plasma treatment time on physical properties and cytotoxicity against cancer cells of *N,O*-carboxymethyl chitosan-stabilized gold nanoparticles (CMC-AuNPs) was investigated. AuNPs were synthesized by chemical reduction of $HAuCl_4$ in 2 % CMC solution to obtain CMC-AuNPs, before being subjected to the plasma treatment. Results showed that the plasma treatment not only led to the reduction of hydrodynamic diameters of CMC-AuNPs from 400 nm to less than 100 nm by the plasma-induced degradation of CMC but also provided the narrow size distribution of AuNPs having diameters in the range of 2–50 nm, that were existing in CMC-AuNPs. In addition, the plasma-treated CMC-AuNPs could significantly reduce the percentage of cell viability of breast cancer cells by approximately 80 % compared to the original CMC and CMC-AuNPs.

1. Introduction

One of the most studied metallic nanoparticles is gold nanoparticles (AuNPs) due to its interesting properties, including biocompatibility, bioconjugation and low toxicity (Arvizo, Bhattacharya, & Mukherjee, 2010; Jain, El-Sayed, & El-Sayed, 2007; Jazayeri, Amani, Pourfatollah, Pazoki-Toroudi, & Sedighimoghaddam, 2016; Nguyen, Park, Kang, & Kim, 2015; Shukla et al., 2005). AuNPs refer to clusters of gold (Au) with diameters ranging from a few to several hundred nanometers (Tréguer-Delapierre, Majimel, Mornet, Duguet, & Ravaine, 2008). Size and shape of AuNPs can be tuned by adjusting synthesis conditions to alter chemical, electrical and optical properties (Tréguer-Delapierre et al., 2008). Surface of AuNPs can be modified to manipulate their charge, hydrophilicity and functionality, leading to specific interactions with cells (Arvizo et al., 2010). When AuNPs enter to a human body, they can be internalized, trafficked, or secreted by various types of cells. In biological fluids, AuNPs can interact with some specific proteins owing to their high surface energy, and this results in the induction of various cellular responses, *e.g.* enhancement of cellular uptakes and immune responses, increase of lysosomal permeability, apoptosis and so on (Boyles et al., 2015; Pengyang et al., 2015; Wang et al., 2011). According to these advantages, AuNPs draw much attention for cancer treatment including imaging, diagnostics, therapies and toxicity (Boisselier & Astruc, 2009; Cai, Gao, Hong, & Sun, 2008; Kim, Jeong, & Jon, 2010; Qiu et al., 2010; Selim & Hendi, 2012). However, in order to obtain the colloidal AuNPs with high stability, some stabilizers such as citrate (Bastús, Comenge, & Puntes, 2011) and CTAB (Fenger, Fertitta, Kirmse, Thünemann, & Rademann, 2012) are required. Recently, some nature-derived stabilizers such as chitosan and chitosan derivatives have been emphasized (Chen et al., 2015; Choi et al., 2012; Thi Lanh et al., 2014), especially in biomedical field, because they are biocompatible and biodegradable, and have some incredible biological properties including anticancer activity (Fernandes et al., 2010; Gibot et al., 2015; Kim, 2010; Xia, Liu, Zhang, & Chen, 2011).

Chitosan is derived from chitin, which is found as a structural constituent in crustacean shells and exoskeleton of insects (Fernández-Martín et al., 2014). Chitosan mainly consists of D-glucosamine units connected by glycosidic linkages and partially inserted by *N*-acetyl-D-

Abbreviations: AuNPs, gold nanoparticles; CMC, *N,O*-carboxymethyl chitosan; CMC-AuNPs, *N,O*-carboxymethyl chitosan-stabilized gold nanoparticles; *DH*, mean hydrodynamic diameter; DS, degree of substitution; PBS, phosphate buffer saline; PDI, polydispersity index; SP, solution plasma; *A*, absorbance; *Mn*, number-average molecular weight; n, number of experiments; ζ, zeta potential

* Corresponding author at: The Petroleum and Petrochemical College, Chulalongkorn University, Bangkok, 10330, Thailand.
E-mail address: ratana.r@chula.ac.th (R. Rujiravanit).

https://doi.org/10.1016/j.carbpol.2020.116162
Received 19 July 2019; Received in revised form 4 March 2020; Accepted 11 March 2020
Available online 12 March 2020
0144-8617/

glucosamine units (Chen et al., 2004). The presence of amino groups at the C2 positions of pyranose rings in chitosan facilitates metal chelation, flocculation and biological properties (Xia et al., 2011). According to accumulated evidences, chitosan oligosaccharides, which are water-soluble degraded products of chitosan, possess anticancer activity against several cancer cell lines (Gibot et al., 2015; Han, Cui, You, Xing, & Sun, 2015; Huang, Mendis, Rajapakse, & Kim, 2006). In general, native chitosan can dissolve in organic acid solutions like acetic acid. However, its solubility in water is very low (El-Sawy, Abd El-Rehim, Elbarbary, & Hegazy, 2010). This limitation hinders chitosan from potential uses in biomedical field. Therefore, production of water-soluble chitosan has drawn much attention from many researchers. Water-soluble chitosan can be obtained from not only degradation but also chemical modification, such as carboxymethylation to obtain carboxymethyl chitosan (CMC) (Chen et al., 2004; Chokradjaroen et al., 2017; El-Sawy et al., 2010; Jiang et al., 2010; Prasertsung, Damrongsakkul, & Saito, 2013). A carboxymethylation reaction of chitosan can occur at hydroxyl groups to form *O*-carboxymethyl chitosan (*O*-CMC), at amino groups to get *N*-carboxymethyl chitosan (*N*-CMC), or at both hydroxyl and amino groups to produce *N*, *O*-carboxymethyl chitosan (*N*,*O*-CMC) (Anitha et al., 2011; Laudenslager, Schiffman, & Schauer, 2008; Shi, Du, Yang, Zhang, & Sun, 2006). An improvement on solubility in water of CMC depends on the degree of substitution of carboxymethyl groups. Although CMC has been used to prepare a drug carrier for anticancer agents (Anitha et al., 2011; Shi et al., 2006), the effect of structural properties, *e.g.* polymer size and degree of substitution, of CMC on the anticancer activity have rarely been reported in literature.

Electrical discharge plasma occurring in a liquid phase, so called solution plasma (SP), was successfully used for degradation of chitosan to obtain low-molecular-weight, water-soluble chitosan (Chokradjaroen, Theeramunkong, Yui, Saito, & Rujiravanit, 2018). SP is generated by immersing a pair of electrodes into a liquid and then electric potential is applied to the electrodes by using a bipolar pulsed power supply (Saito, Hieda, & Takai, 2009). SP can be operated at atmospheric pressure and room temperature, and generate several highly active species (*e.g.* $H_2O \rightarrow {}^{\cdot}OH + {}^{\cdot}H$) (Baroch, Anita, Saito, & Takai, 2008). These highly active species can promote a variety of chemical reactions with less chemicals used or without chemicals; for instance, degradation of organic compounds (Baroch et al., 2008) and biopolymers by using chemicals less than conventional methods (*i.e.* acid hydrolysis and oxidative degradation) (Prasertsung et al., 2013; Watthanaphanit & Saito, 2013), and synthesis of metal and carbon nanoparticles without the addition of chemical agents (Kang, Li, & Saito, 2013; Takai, 2014). Accordingly, the highly reactive species generated by SP can possibly involve in degradation of biopolymers used to stabilize metal nanoparticles, aiming to reduce chemical uses for the purpose of biomedical applications.

In this study, AuNPs were synthesized by a chemical reduction of $HAuCl_4$ dissolved in a CMC solution using $NaBH_4$ as a reducing agent in order to obtain a stable colloidal suspension of CMC-stabilized AuNPs (CMC-AuNPs), aiming to evaluate the cytotoxicity of CMC-AuNPs against different types of cancer cells. Furthermore, both CMC and CMC-AuNPs were subjected to the SP treatment to induce chain scission of CMC and size reduction of AuNPs. Thereafter, the influence of hydrodynamic sizes of CMC-AuNPs before and after the SP treatment on the cytotoxicity against cancer cells was investigated. The cytotoxicity against cancer cells was determined by MTT assay and the pathway of cell death was identified by flow cytometry analysis.

2. Experimental

2.1. Synthesis of CMC-AuNPs

Details on materials used in this study as well as the synthesis method and characterization of CMC are described in supplementary data. The synthesized CMC (2 g) was dissolved in DI water (80 mL). $HAuCl_4$ was dissolved in DI water to prepare a stock solution at a concentration of 10 mM. The stock solution of $HAuCl_4$ was diluted and mixed with the CMC solution to obtain the final concentrations of $HAuCl_4$ at 0.05, 0.2 and 2 mM and the final volume of 100 mL, followed by stirring at room temperature for 1 h. Then, the obtained solution was gradually poured into the alkaline solution (200 mL) containing 2 M NaOH and $NaBH_4$ (0.1 g) with vigorous stirring and then left overnight at room temperature. After that, an excess amount of acetone was added to the solution and left at 4 °C for 24 h to precipitate the CMC-stabilized AuNPs (CMC-AuNPs). The precipitate was collected by centrifugation at 12,000 rpm for 10 min and washed three times by the mixture of acetone and water at a ratio of 9:1. Finally, the obtained products were re-dissolved in DI water prior to freeze-drying and the freeze-dried products were kept in a desiccator for further use.

2.2. SP treatment of CMC and CMC-AuNPs

CMC and CMC-AuNPs (0.5 g) were dissolved in DI water (50 mL) to prepare the reaction solutions. Then, the reaction solution was poured into a plasma reactor, which was adapted from a glass beaker equipped with a pair of 1 mm-diameter tungsten electrodes (purity 99.9 %, Nilaco Corp., Japan), and kept stirring during the plasma discharge in order to provide the uniformity of the solution inside the reactor. The

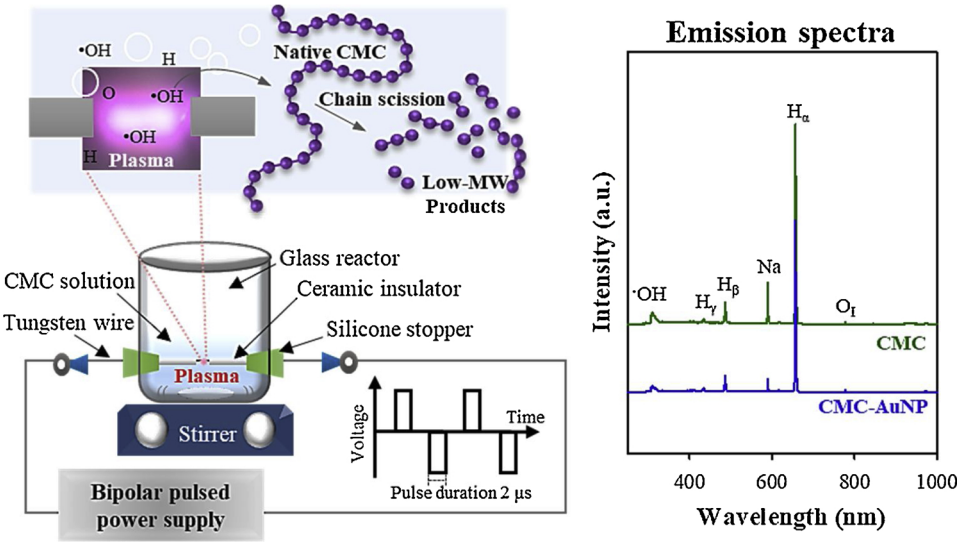

Fig. 1. Experimental setup of SP and optical emission spectra (OES) for the SP treatment of CMC and CMC-AuNPs solutions.

experimental set-up of SP is shown in Fig. 1. The plasma discharge occurred at the tips of the tungsten electrodes that were connected to a bipolar pulsed power supply (Kurita-Nagoya MPS-06K06C, Kurita Co. Ltd., Japan). The electrodes were submerged in the reaction solution and the distance between the electrodes was adjusted to be 0.75 mm. The operating condition of the plasma treatment was fixed at the frequency, voltage and pulse width of 15 kHz, 1.6 kV and 2 μs, respectively.

2.3. Characterization

A 500-MHz nuclear magnetic resonance spectroscopy or NMR (AVANCE III, Bruker) was used to determine the chemical structures of native chitosan and CMC products. Chitosan and CMC were dissolved in CD_3COOD/D_2O and D_2O, respectively, at a concentration of 10–30 mg/mL. The chemical composition and chemical structure were investigated by using X-ray photoelectron spectroscopy or XPS (Kratos Axis Ultra DLD) and Fourier transform infrared spectroscopy or FT-IR (Nicolet iS5, Thermo Fisher Scientific). XPS with a monochromatic Al Kα as an X-ray source (anode HT = 15 kV) was used. The C—C peak in the C 1s region was applied as an internal standard (284.6 eV) to calibrate the binding energies of all elements. High resolution XPS traces were deconvoluted by Origin Pro 2016 software. For creating baselines, the 2nd Derivative method was used for locating anchor points and the spline method was selected as interpolation method. The baseline was subtracted from a spectrum prior to the peak-fitting. For FT-IR, the 64 scans with a correction for atmospheric carbon dioxide (CO_2) were used as the operating condition. The measured results were interpreted by using OMNIC FT-IR Software. Carbon, hydrogen and nitrogen compositions of native chitosan and CMC were analyzed by using CHN elemental analyzer (Perkin Elmer analyzer model 2400, PerkinElmer). The crystal structures of CMC and CMC-AuNP was determined by X-ray diffraction or XRD (SmartLab, Rigaku) with Cu Kα radiation in a continuous mode. The formation of AuNPs was monitored by observing optical property of the solutions of CMC-AuNP with a UV–vis spectrophotometer (UV-1800, Shimadzu) in the spectral range from 400 to 800 nm. The samples were prepared by 3-fold dilution prior to the measurement. The morphology of the freeze-dried CMC-AuNP was investigated by field emission scanning electron microscopy or FE-SEM (JSM-7610F, JEOL) equipped with energy dispersive X-ray spectroscopy (EDS). The particle shape and size of AuNPs were determined based on transmission electron microscopy or TEM (JEM-2000EX, JEOL). Zeta potential measurement of the AuNPs was carried out using a zeta potential analyzer (Zetasizer Nano ZS, Malvern Instruments). Dynamic light scattering or DLS (Zetasizer Nano ZS, Malvern Instruments) was used to measure the hydrodynamic sizes of CMC and CMC-AuNPs before and after the SP treatment at a concentration of 0.2 mg/mL. All samples were measured for three times (n = 3). The changes in an average molecular weight of CMC were investigated by gel permeation chromatography or GPC (Shimadzu), equipped with a refractive index (RI) detector. The ultrahydrogel linear column (Water 600E, Waters) for separation of molecular weight in the range of 1.0×10^3–2.0×10^7 Da was connected in series with a guard column equipped in an oven at the operating temperature of 30 °C. The mobile phase was a 0.5 M sodium bicarbonate buffer solution at pH 11 and the flow rate was set at 0.6 mL/min. The injection volume of a sample was 20 μL comprising of 2 mg/mL CMC in the buffer solution. Pullulans with molecular weights in the range of 5.9×10^3–7.0×10^5 Da were used as standards.

2.4. Biological tests

Cell cultures of cancer and normal cells were described in supplementary data. The cytotoxicity of the test samples was conducted by using MTT (3-(4,5-dimethylthiazol-2-yl)-2,5-diphenyltetrazolium bromide) assay. Cells were seeded into 96-well microliter plates (1×10^4 cells/well). After 24 h, cells were treated with different concentrations of the samples, diluted with sterile water to make the desired final concentration (0.065–1 mg/mL). Then, the treated cells were incubated in an incubator at 37 °C and 5% CO_2 for 24 h. After incubation, the medium was replaced with a PBS (phosphate buffer saline) solution containing 0.05 % w/v of MTT solution and further incubated for 3 h. The solution was then discarded and DMSO was added to dissolve the formed formazan crystals. The absorbance (A) of each well was measured at 570 nm using a microplate reader (Varioskan™ Flash Multimode Reader, Thermo Fisher Scientific). All experiments were performed in triplicate and repeated for five experiments (n = 5). The cell viability of the cells that were treated by the obtained samples was expressed as a percentage relative to the untreated control cells as follow:

$$\text{Cell viability (\%)} = 100 \times |(A_{\text{treated}} - A_{\text{blank}})/(A_{\text{untreated}} - A_{\text{blank}})| \quad (1)$$

After the percentage of cell viability was calculated and plotted as a function of sample concentrations, the concentration that 50 % of the cell population was killed in a given period of time (IC_{50}) was determined. All the data presented were expressed as average ± standard deviation, and the statistical analysis was done by using one-way ANOVA in JMP Pro 14 program. The difference was considered statistically significant when the p value was less than 0.05.

Wound healing assay was also performed to examine the cell maintenance after being damaged. The cells were cultured in a 96-well plate until reaching confluence. After that, the cells were scratched by a plastic pipette tip across the center of the plates to produce a wound area. The scratched cells were treated with the test sample before culturing for 72 h. The images of the cells were taken immediately and every hour for 72 h after being scratched and treated with a test sample. Moreover, the induction of apoptosis in MCF-7 cells, a breast cancer cell line, by the test sample was examined by FITC-labeled annexin V (FITC-annexin V) staining of the treated cells. The treated cells were harvested and washed with cold PBS twice. The cells were then stained with FITC-annexin V-PI as indicated in manufacturer's instruction (FITC Annexin V Apoptosis Detection Kit, BD Pharmingen, USA) and analyzed in a BD FACS Verse™ (BD Biosciences) flow cytometer. The data were collected with BD FACSuite™software for 10^4 cells in each sample. A parallel set of FITC-annexin V-PI stained cells was also visualized for apoptosis under In Cell analyzer (In Cell analyzer 2000, GE Healthcare Life Sciences) under bright field and fluorescence modes.

3. Results and discussion

3.1. Characterization of CMC-AuNPs before and after SP treatment

The CMC that was used to stabilize AuNPs was *N,O*-CMC having degree of substitution (DS) of 0.76 and number-average molecular weight (M_n) of 160 kDa. The colloidal suspension of CMC-AuNPs were synthesized by the chemical reduction of $HAuCl_4$ solutions having different final concentrations of 0.05, 0.2 and 2 mM in the CMC solution having a final concentration of 2 % (w/v) and the obtained products were assigned as CMC-AuNP1, CMC-AuNP2 and CMC-AuNP3, respectively. The absorption spectra of CMC-AuNPs were determined by a UV–vis spectrophotometer using a wavelength scan mode (Fig. 2). The absorption band of AuNPs existing in the CMC-AuNPs was found at the wavelength of 510–520 nm, which was in good agreement with the previous studies (Kannan, Los, Los, & Niedziolka-Jonsson, 2014; Watthanaphanit, Panomsuwan, & Saito, 2014). The absorption band of AuNPs generally depends on size and shape of AuNPs. For example, the rod-shaped AuNPs has the absorption band with two maximum wavelengths (λ_{max}) while the sphere-shaped AuNPs shows only one λ_{max} (El-Brolossy et al., 2008). Therefore, it might be implied that the synthesized AuNPs existing in the CMC-AuNPs had the spherical shape. The absorption spectra of CMC-AuNP1, CMC-AuNP2 and CMC-AuNP3 show

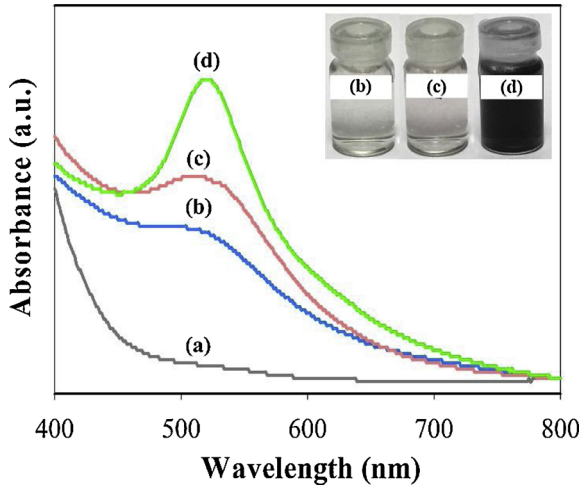

Fig. 2. UV–vis absorption spectra of (a) the original CMC, (b) CMC-AuNP1 (0.05 mM $HAuCl_4$), (c) CMC-AuNP2 (0.2 mM $HAuCl_4$) and (d) CMC-AuNP3 (2 mM $HAuCl_4$).

the absorption bands with the λ_{max} at 510, 517 and 520 nm, respectively. The shift of λ_{max} to the longer wavelength when the $HAuCl_4$ concentrations were increased indicated the increasing of the particle sizes of AuNPs (Watthanaphanit et al., 2014). From the XRD analysis (Fig. S2 in Supplementary data), it was found that the average crystalline sizes of AuNPs existing in CMC-AuNP2 and CMC-AuNP3 were calculated to be 14.2 and 27.1 nm, respectively. Moreover, the formation of AuNPs existing in CMC-AuNPs was also confirmed by FE-SEM equipped with EDS (Fig. S3 in the Supplementary data).

The particle size and size distribution of the AuNPs existing in the CMC-AuNPs before and after the SP treatment were determined by TEM (Fig. 3). It was found that the concentrations of gold precursor, *i.e.* $HAuCl_4$, had an influence on the particle size and size distribution of CMC-AuNPs. The average particle sizes of AuNPs existing in CMC-AuNP1, CMC-AuNP2 and CMC-AuNP3 were 6, 11 and 24 nm, respectively (Fig. 3(A)–(C)), indicating the aggregation of AuNPs when the concentrations of $HAuCl_4$ were increased from 0.05 mM to 0.2 and 2 mM, respectively. The results suggested that 0.2 mM of $HAuCl_4$ seemed to be an optimal concentration for synthesis of CMC-AuNPs because the obtained CMC-AuNP2 had relatively low aggregation compared to CMC-AuNP3 and contained higher amount of AuNPs than CMC-AuNP1. Therefore, CMC-AuNP2 was chosen for further investigation on the effect of the SP treatment. After the SP treatment, the TEM images of the SP-treated CMC-AuNP2 revealed that the size distribution of AuNPs existing in the SP-treated CMC-AuNP2 became narrower and the particle size of AuNPs was slightly smaller when the SP treatment time increased from 0 min to 45 and 90 min (Fig. 3(D), (E)). The average particle sizes of AuNPs existing in the SP-treated CMC-AuNP2 after the SP treatment for 45 and 90 min, which were designated as CMC-AuNP2SP45 and CMC-AuNP2SP90, were equal to 10 and 9 nm, respectively. Similarly, Saito and co-workers (Saito et al., 2009) investigated the synthesis of AuNPs by the SP treatment and reported that the particle size of AuNPs became smaller as prolonging the SP treatment time. The longer SP treatment time could lower the pH of the reaction solution, leading to partial dissolution of AuNPs. According to the FT-IR results (Fig. S4 in Supplementary data), the chemical structures of the SP-treated CMC and the SP-treated CMC-AuNP2 did not change after the SP treatment. The change to the smaller size of AuNPs after the SP treatment may be considered as a merit of the SP treatment, because this can lead to broaden utilization of AuNPs, especially in medical application, in which the particle size of AuNPs is an important factor. Nanoparticles with a size smaller than 100 nm can facilitate cellular uptakes of nanoparticles and nanoparticles with a size of 2–6 nm could locate in not only cytoplasm but also nucleus (Huang et al., 2012; Xu et al., 2012). Moreover, the distribution of nanoparticles, such as AuNPs, in tissues and organs was also reported to be size dependent. According to the literature, AuNPs with a size smaller than 50 nm could pass blood–brain barrier as evidenced by the presence of AuNPs in the brain of the tested mice after intravenous administration for 24 h (Sonavane, Tomoda, & Makino, 2008). This indicated that the smaller size of AuNPs results in the higher opportunity that AuNPs can pass through various target cells.

Stability of nanoparticles plays an important role in their utilization for medical application. Single and aggregated nanoparticles can result in different cellular responses. For instance, the decreases in cellular uptakes of aggregated nanoparticles by HeLa and A549 cells were reported in comparison to single and monodisperse nanoparticles (Albanese & Chan, 2011). The stability of the synthesized CMC and CMC-AuNPs was investigated by zeta potential measurement. Zeta potential (ζ) of the synthesized CMC and CMC-AuNPs before and after the SP treatment are demonstrated in Table 1. ζ can be used to predict a potential stability of particles in suspensions (Nivethaa, Dhanavel, Narayanan, Vasu, & Stephen, 2015). In general, a suspension with ζ less than −30 mV and more than +30 mV is considered as a stable suspension (Watthanaphanit et al., 2014). In the absence of AuNPs, the ζ of CMC solution at neutral pH was −51 mV. The minus value indicated the negatively charged nature of CMC (Kalliola et al., 2017). The ζ of CMC-AuNPs ranged from –40 to −50 mV, suggesting that the CMC could provide a good stabilization to AuNPs. However, the ζ values were found to be shifted to zero side by reducing their negative magnitudes as increasing the amount of AuNPs. The decrease in the ζ magnitudes may be attributed to less stable colloid, which indicates the aggregation or the increase in particle size. Theoretically, the stability of nanoparticle system depends on the balance of attractive and repulsive forces (Tantra, Schulze, & Quincey, 2010). When the repulsive force between nanoparticles is greater than attractive force, the colloid remains stable. At the diluted concentration of nanoparticles, the separation distance between particles increases, leading to the reduction of attractive forces between particles. On the other hand, at the higher concentration of nanoparticles, the separation distance between nanoparticles becomes closer, resulting in the increment of the attractive forces. Moreover, when the number of nanoparticles increases, the charged molecules and ions existing in the system, which facilitate the electrostatic stabilization, may be absorbed on the surface of nanoparticles (Medrzycka, 1991), causing the instability of nanoparticles. To investigate the absorption of the CMC on the surface of AuNPs, DLS measurement was performed and the results are shown in Table 1. The hydrodynamic diameters (D_H), which can refer to a macromolecule size in a solution, of the CMC-AuNPs decreased when the amount of AuNPs increased. This might be implied that some parts of the polymer chains might wrap around AuNPs (Haesuwannakij et al., 2017), leading to the shrinkages of polymer chains in the solution. Hence, the shrinkage of polymer chains might shorten the separation distance between nanoparticles, resulting in the increment of the attractive forces, and eventually the reduction of stability.

Further investigation on the suspensions of the SP-treated CMC and CMC-AuNPs revealed that the SP treatment caused the reduction of their negative magnitudes of ζ (Table 1). Since the SP treatment generally generates some highly reactive species (Saito, Bratescu, & Hashimi, 2017), these highly reactive species might interact with the CMC and CMC-AuNPs. However, the ζ of the SP-treated CMC and CMC-AuNPs (*i.e.* –26 to −34 mV) were still in the acceptable range for achieving good stability. In addition, for the stabilization of AuNPs by using CMC, not only electrostatic but also steric stabilization should be considered, because CMC is a long-chain polymer. The steric stabilization usually depends on molecular weight of polymers (Heller & Pugh, 1960). High-molecular-weight polymers can greatly form entanglement, which can hinder the attractive forces between nanoparticles, resulting in less aggregation of nanoparticles (Choi, Park, & Lee, 2008). According to the DLS measurement, the hydrodynamic

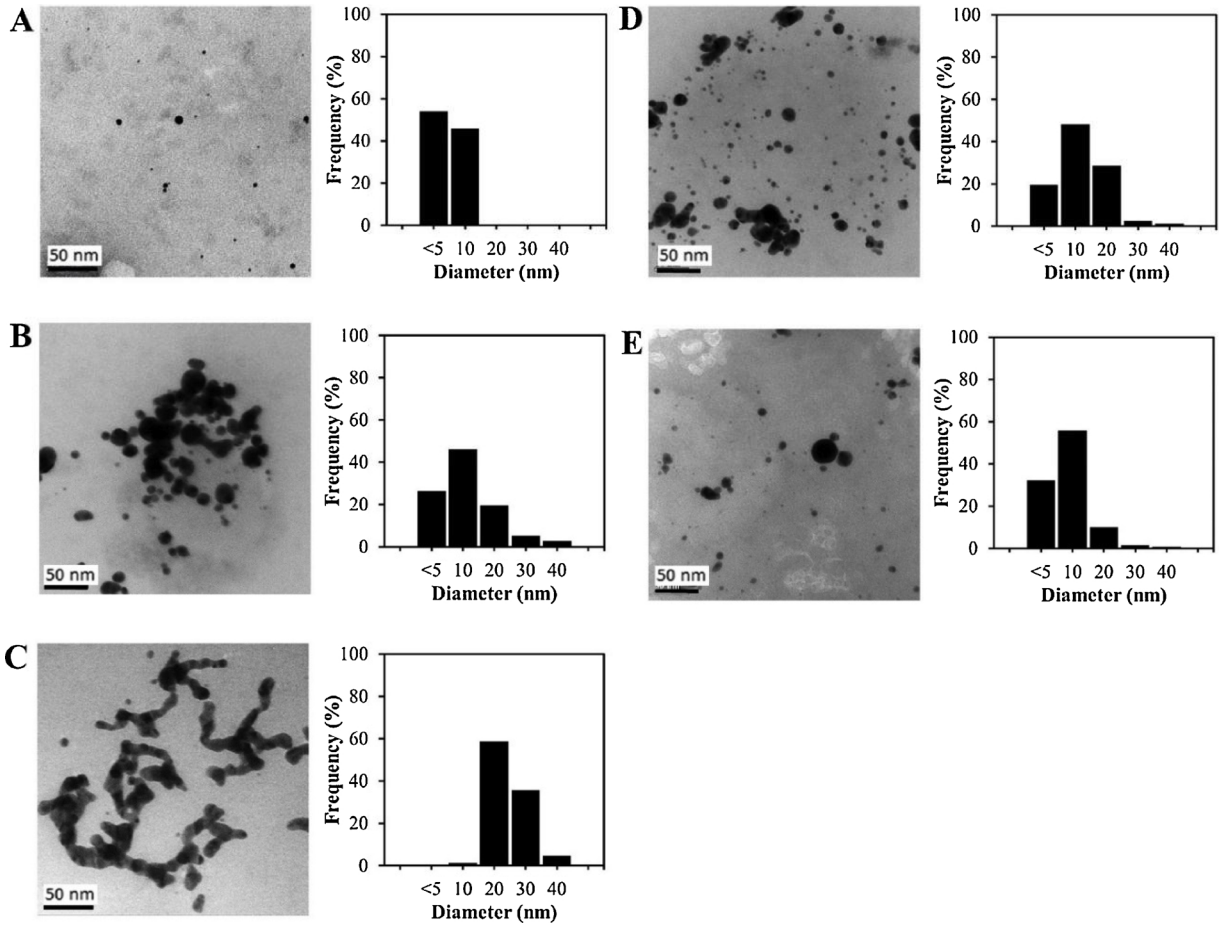

Fig. 3. TEM images of (A) CMC-AuNP1, (B) CMC-AuNP2 and (C) CMC-AuNP3 and the SP-treated CMC-AuNP2 after the SP treatment for (D) 45 min (CMC-AuNP2SP45) and (E) 90 min (CMC-AuNP2SP90).

Table 1
Number-average molecular weight (M_n) of the original and the SP-treated CMC and mean hydrodynamic diameter or *Z*-average (D_H) and zeta potential (ζ) of the CMC and CMC-AuNPs by using various concentrations of $HAuCl_4$ before and after the SP treatment.

Samples	[$HAuCl_4$] (mM)	SP treatment time (min)	M_n *(kDa)	D_H (nm) {PDI}	ζ (mV)
CMC	0	0	160	410 ± 60 {0.65}	–51 ± 3
CMCSP45		45	85	330 ± 70 {0.67}	– 44 ± 3
CMC-SP90		90	34	239 ± 33 {0.66}	–32 ± 4
CMC-AuNP1	0.05	0	n/a	433 ± 100 {0.56}	–51 ± 1
CMC-AuNP2	0.2	0	n/a	105 ± 9 {0.56}	–43 ± 2
CMC-AuNP2SP45		45	n/a	57 ± 1 {0.61}	–32 ± 2
CMC-AuNP2SP90		90	n/a	30 ± 3 {0.76}	–26 ± 1
CMC-AuNP3	2	0	n/a	71 ± 1 {0.50}	–40 ± 1

Note: *M_n values were obtained from the GPC measurement. PDI refers to polydispersity index.

diameter (D_H) of both SP-treated CMC and CMC-AuNPs decreased, which could refer to the reduction of molecular weight of CMC (Table 1). Some highly reactive species produced in the SP system could cause chain scission of the CMC at β-glyosidic linkages with low impact to its functional groups (Chokradjaroen et al., 2017). Therefore, the SP-treated CMC and CMC-AuNPs, which had lower molecular weight, possibly formed less entanglement than that occurred in the SP-untreated CMC and CMC-AuNPs, resulting in lower stability of the samples. Nevertheless, the smaller hydrodynamic diameters of the SP-treated CMC and CMC-AuNPs may lead to a benefit. As mentioned previously, particles with sizes smaller than 100 nm could accomplish better cellular uptakes (Huang et al., 2012). Accordingly, CMC-AuNP2SP45 and CMC-AuNP2SP90, having D_H of 57 and 32 nm, may have potential for medical utilization.

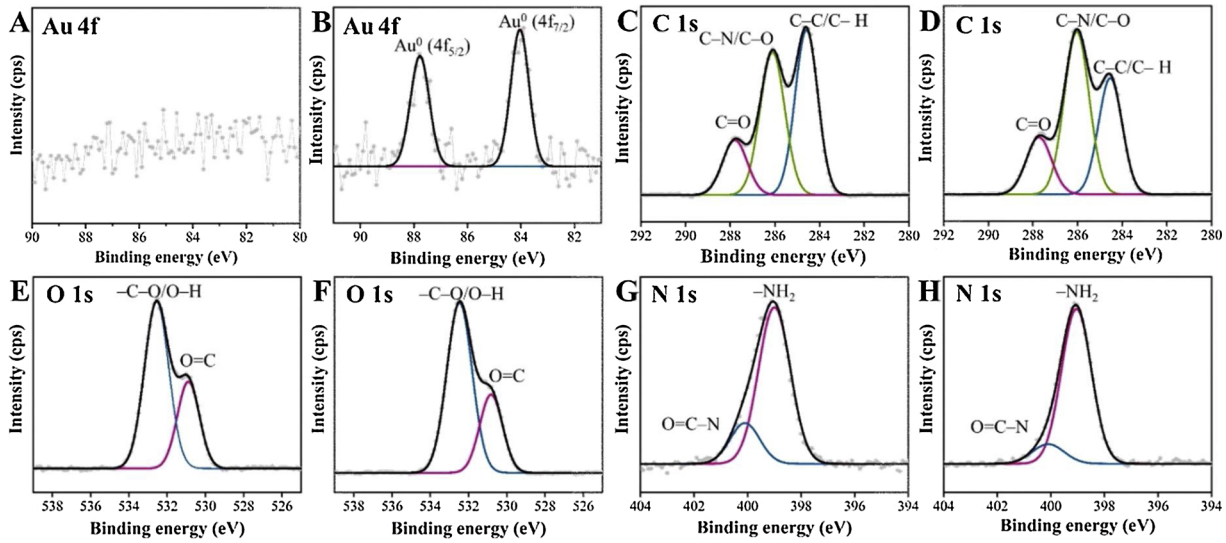

Fig. 4. XPS spectra of the synthesized CMC, showing peaks of (A) Au 4f, (C) C 1s, (E) O 1s, and (G) N 1s, and CMC-AuNP2, showing peaks of (B) Au 4f, (D) C 1s, (F) O 1s, and (H) N 1s.

The chemical compositions of CMC and CMC-AuNP2 were examined by XPS (Fig. 4). Compared with the XPS spectrum of CMC, the new peaks at 83.9 and 87.4 eV, corresponding to the binding energy of AuNPs, is observed in the XPS spectrum of the CMC-AuNP2 (Kang, Qu, Alvarez, & Zhu, 2017). Other components, including C 1s, O 1s and N 1s, were also characterized in order to investigate their interaction with CMC after the chemical reduction of Au^{3+} to AuNPs in the CMC solution. For the CMC, the C 1s peaks at 284.6, 286.1 and 287.8 eV are attributed to C—C/C—H, C—N/C—O and C═O bonds, respectively (Hu, Chen, Feng, Hu, & Liu, 2016; Li et al., 2016). The C 1s spectrum of CMC-AuNP2 displayed a significant decrease in C—C/C—H, which might indicate a possible intimate contact of AuNPs with —CH in pyranose rings (Silva et al., 2013). Moreover, CMC-AuNP2 showed a lower binding energy of C═O in the O 1s spectra than that obtained from the original CMC. This might be a result from coordination of AuNPs and carboxyl groups of CMC. The N 1s of the CMC and CMC-AuNP2 were also examined (Serro et al., 2006). However, there was a slight change in the peak of O═C—N, which should belong to some remaining acetamido groups in CMC. The interaction between AuNPs and CMC was also supported by the evidence from FT-IR (Fig. S4 in Supplementary data). The FT-IR spectra of the CMC-AuNPs revealed the decrement of the peak at 1650 cm^{-1}, corresponding to —COO of a sodium form of CMC, compared to that of the original CMC. This alteration was also found in the previous study, which was suggested to be a result from the interaction between the carboxyl groups of CMC and the metal atoms (Gu, Sun, Wu, Wang, & Zhu, 2007; Karaoğlu, Baykal, Şenel, Sözeri, & Toprak, 2012).

Moreover, the XPS measurement was also used to investigate the changes in the chemical structure of the CMC-AuNPs after the SP treatment. The XPS spectra (*i.e.* Au 4f and O 1s), shown in Fig. S5 in the Supplementary data, reveals that the intensity of the peak at 532.7 eV, attributed to C—O—C, decreased, which might be due to the oxidative degradation by the SP-induced ˙OH, leading to the chain scission at β-glycosidic linkages of CMC. Meanwhile, the peak of Au 4f, corresponding to the gold metal in AuNPs, suggested that there was no gold oxide formation, *e.g.* Au_2O_3, after the SP treatment. However, the peak of Au $4f_{7/2}$ of AuNPs existing in the CMC-AuNPs shifted from 83.8 eV to a higher binding energy of 84.2 eV. This phenomenon might be due to the electron transfer occurring through the interaction between the AuNPs and the oxygen-containing functional groups in the surrounding SP-treated CMC. Accordingly, it is possible that the shorter chain of CMC could interact and wrap around the AuNPs, which could prevent the aggregation and maintain the stability of the AuNPs, even though the SP-treated CMC had lower molecular weight than the original CMC.

Fig. 5 shows a proposed mechanism for the formation of the CMC-AuNPs with a smaller D_H by the SP treatment. Firstly, gold cations, Au^{3+}, formed a chelation with the negative charge of CMC (*i.e.* a carboxymethyl group), which is similar to the chelation between carboxylic acids, such as citric acid, and metal nanoparticles (Erdemi, Baykal, Karaoğlu, & Toprak, 2012; Uznanski, Zakrzewska, Favier, Kazmierski, & Bryszewska, 2017). When Au^{3+} was reduced to form AuNPs, the AuNPs possibly form coordination with the carboxymethyl groups of CMC, which resulted in the reduction of negative magnitude of ζ compared with that of the original CMC. In addition, as evidenced from the FT-IR and XPS analyses, the AuNPs could possibly interact with the —CH in pyranose rings, in which a hydroxyl group is attached to this carbon. After that, the suspension of CMC-AuNPs was subjected to the SP treatment, which could induce the ionization of water molecules to produce highly reactive species (*i.e.* ˙OH and ˙H) (Potocký, Saito, & Takai, 2009). The formation of highly reactive species, which have been previously reported that they could involve in the degradation of chitosan at its β-glycosidic linkages (Pornsunthorntawee, Katepetch, Vanichvattanadecha, Saito, & Rujiravanit, 2014; Prasertsung, Damrongsakkul, Terashima, Saito, & Takai, 2012, 2013), was detected by optical emission spectroscopy (OES) measurement (Fig. 1). Therefore, it might be explained that the generated ˙OH and ˙H involved in the chain scissions of CMC and CMC-AuNPs at the glycosidic linkages of CMC during the SP treatment, leading to the reduction of M_n and D_H of CMC and CMC-AuNPs, respectively.

3.2. Biological tests

Table 2 shows the results from cytotoxicity test on the cell viability of MCF-7 cells after being treated with the original CMC and CMC-AuNPs (*i.e.* CMC, CMC-AuNP1, CMC-AuNP2 and CMC-AuNP3), and the SP-treated CMC and CMC-AuNPs (*i.e.* CMC-SP90, CMC-AuNP2SP45 and CMC-AuNP2SP90). It was found that the original CMC alone did not show significant inhibitory effect toward MCF-7 cells. Even though MCF-7 cells were treated with the CMC-AuNP1, CMC-AuNP2 and CMC-AuNP3, the percentages of cell viability of the treated MCF-7 cells were still high, *i.e.* 89.9 %, 89.6 % and 84 %, respectively. According to the literatures, it has been reported that AuNPs are non-toxic (Brown et al., 2010; Pengyang et al., 2015). However, due to their high surface energy, AuNPs may have interactions with some proteins that are probably recognized by cell membrane receptors, resulting in more specific binding to cells, and consequently facilitating cellular uptakes (Oh

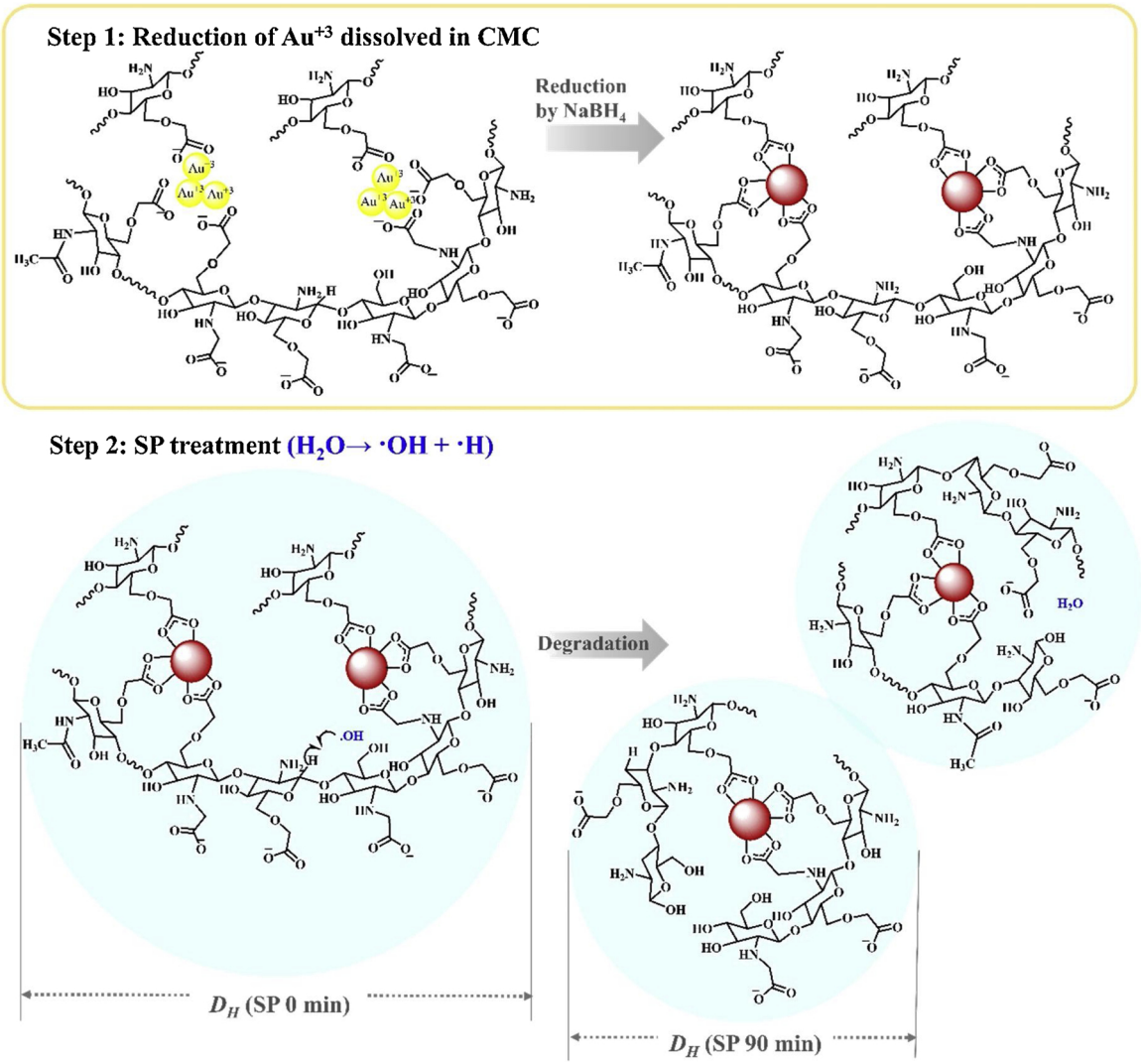

Fig. 5. Illustration of the reduction of Au^{3+} to form AuNPs in the CMC solution and a proposed mechanism for the formation of CMC-AuNPs with a smaller D_H by the SP-induced degradation of CMC (Note: D_H means hydrodynamic diameter).

Table 2
Cytotoxicity against MCF-7 cells of CMC and CMC-AuNPs before and after the SP treatment at the concentration of 0.5 mg/mL and cultivation time of 24 h (*$p < 0.05$, as compared between different samples).

Samples	[$HAuCl_4$] (mM)	SP treatment time (min)	Cell viability (%)
CMC	0	0	91.5 ± 3.5
CMC-SP90		90	89.0 ± 6.4
CMC-AuNP1	0.05	0	89.9 ± 5.2
CMC-AuNP2	0.2	0	89.6 ± 3.3
CMC-AuNP2SP45		45	27.3 ± 4.7*
CMC-AuNP2SP90		90	17.3 ± 1.9*
CMC-AuNP3	2	0	84.0 ± 4.6

et al., 2011). For this reason, the CMC-AuNPs had higher potential to be absorbed by cells, leading to higher biological activities than CMC alone.

Furthermore, when the amount of AuNPs existing in CMC-AuNPs increased, CMC-AuNP3 possessed the higher cytotoxicity against MCF-7 cells than CMC-AuNP1 and CMC-AuNP2. The results from DLS measurement indicated that the increasing of the amount of AuNPs in CMC-AuNPs led to the decrease in D_H of CMC-AuNPs (Table 1). It is well-known that not only quantity of nanomaterials but also other characteristics of nanomaterials, especially size, affect their functions in biological systems. In case of biopolymers like chitosan and proteins, a smaller size usually results in the enhancement of their biological activities and cellular uptakes (Boyles et al., 2015; Pengyang et al., 2015). Among the studied CMC-AuNPs, *i.e.* CMC-AuNP1, CMC-AuNP2 and CMC-AuNP3, CMC-AuNP3 had the smallest value of D_H, *i.e.* 71 nm, and the highest amount of AuNPs. However, some aggregation of CMC-AuNP3 could be observed, as evidenced by its TEM image (Fig. 3(C)). The aggregation might reduce cellular uptake of CMC-AuNP3, resulting in lowering of cellular responses. Accordingly, the cytotoxicity of CMC-AuNP3 against MCF-7 cells was low. Owing to the aggregation of CMC-AuNP3, CMC-AuNP2 having D_H of 105 nm was used for further study. CMC-AuNP2 was subjected to the SP treatment for 45 and 90 min and the SP-treated products were designated to be CMC-AuNP2SP45 and CMC-AuNP2SP90, respectively. By the SP treatment, the D_H of CMC-AuNP2 was reduced to be 57and 30 nm for CMC-AuNP2SP45 and CMC-AuNP2SP90, respectively. Since the smaller size particles can facilitate cellular uptakes and enhance cellular responses, the reduction of D_H after the SP treatment led to the better cytotoxic effect. For this reason, CMC-AuNP2SP90, which had the smallest D_H, *i.e.* 30 nm, showed the highest cytotoxicity against MCF-7 cells, compared to CMC-AuNP2 and CMC-AuNP2SP45 which had D_H of 105 and 57 nm, respectively.

Subsequently, CMC-AuNP2SP90 was further evaluated for its cytotoxicity against other cancer cells, including HeLa and H460 cells, as

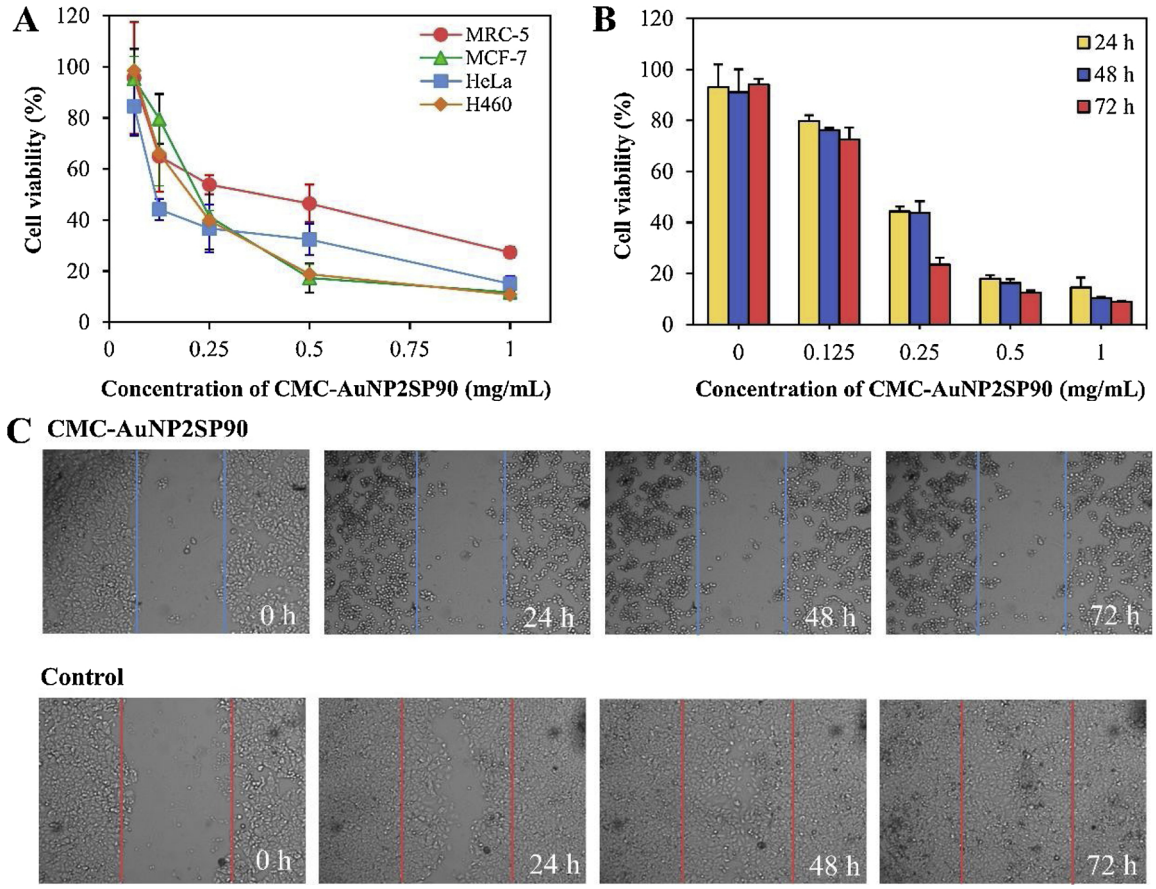

Fig. 6. (A) Cytotoxicity of CMC-AuNP2SP90 against various types of cancer cells, *i.e.* MCF-7, Hela and H460, in comparison with the normal cell (MRC-5) at cultivation time of 24 h ($p < 0.05$, as compared between different concentrations). (B) Cytotoxicity of CMC-AuNP2SP90 against MCF-7 cells as a function of concentrations of CMC-AuNP2SP90 at different cultivation times ($p > 0.05$, as compared between different cultivation times). (C) Wound healing of MCF-7 cells treated and untreated (control) with CMC-AuNP2SP90 as a function of cultivation times.

well as MRC-5 cells that are the normal cells of human fibroblasts from lung tissue (Fig. 6(A)). It was found that the half maximal inhibitory concentrations (IC_{50}) of CMC-AuNP2SP90 against MCF-7, HeLa, H460 and MRC-5 cells were 0.21, 0.12, 0.20 and 0.42 mg/mL, respectively, indicating that CMC-AuNP2SP90 had higher cytotoxicity toward the cancer cells than the normal cell, but not obvious significant. Cancer cells typically experience changes in their metabolic programs for their adenosine triphosphate (ATP) needs, such as increased uptake rate of glucose, in order to adapt their metabolisms to survive and multiply under the cancer microenvironment (Fadaka et al., 2017). Perhaps, the repeating unit of CMC has chemical structure similar to glucose; therefore, this might be a reason that the CMC-AuNPs with a small D_H could undergo faster cellular uptake and possessed stronger biological activity against the cancer cells than the normal cells (Uldry, Ibberson, Hosokawa, & Thorens, 2002). However, when CMC-AuNP2SP90 was compared to a chemotherapy agent, *i.e.* doxorubicin (Fig. S6 in the Supplementary data), the results revealed that CMC-AuNP2SP90 resulted in the higher cell viability for both cancer and normal cells than that obtained after treating the cells with doxorubicin. Even though CMC-AuNP2SP90 showed the lower cytotoxicity against MCF-7, compared to doxorubicin, CMC-AuNP2SP90 exhibited the lower cytotoxicity against the normal cells as well. Furthermore, the cytotoxic effect of CMC-AuNP2SP90 was found to be concentration-dependent. The percentages of cell viability were greatly reduced at the high concentrations of CMC-AuNP2SP90.

In addition, the effects of concentrations of CMC-AuNP2SP90 and cultivation time on the cell viability of MCF-7 cells treated with CMC-AuNP2SP90 were examined (Fig. 6(B)). It was found that the cell viability of MCF-7 cells, being treated with CMC-AuNP2SP90, decreased with the increasing of concentrations of CMC-AuNP2SP90. On the other hand, there was a slight change on the cell viability of MCF-7 cells when the cell cultivation time was prolonged. Additionally, Fig. 6(C) depicts the development and maintenance of the MCF-7 cells treated with CMC-AuNP2SP90, compared to that of untreated cells (control). The CMC-AuNP2SP90-treated MCF-7 cells could not recover from the wound while the untreated cells could fully recover after 48 h. The result suggested that the higher concentration of CMC-AuNP2SP90 and longer treatment time might promote the cellular uptake and accumulation of CMC-AuNP2SP90 in the cells, leading to cell death.

A pathway of cell death was also investigated by the annexin V/PI assay on MCF-7 cells after being treated with CMC-AuNP2SP90 at concentrations of 0.125 and 0.25 mg/mL for 24 h (Fig. 7(A)). CMC-AuNP2SP90 at the concentration of 0.25 mg/mL could encourage early apoptosis of MCF-7 cells for 20.3 %, late apoptosis for 17.5 % and necrosis for 1.7 %. Moreover, MCF-7 cells treated with CMC-AuNP2SP90 at the concentration of 0.25 mg/mL were further analyzed by using fluorescence microscopy (Fig. 7(B)). Some CMC-AuNP2SP90-treated cells were positive for both annexin V and PI, implying that the cells exhibited apoptotic features. Apoptosis is a programmed cell death for normal cells to keep the organism alive and adapt to surroundings, while cancer cells normally show the loss of apoptosis regulation (Han et al., 2015). However, the mechanism of the synergistic effect of CMC and AuNPs after the SP treatment on apoptotic cell death of cancer cells requires further studied for better understanding of the action of the SP-treated CMC-AuNPs in living cells.

As mentioned above, the SP treatment could induce the cytotoxicity

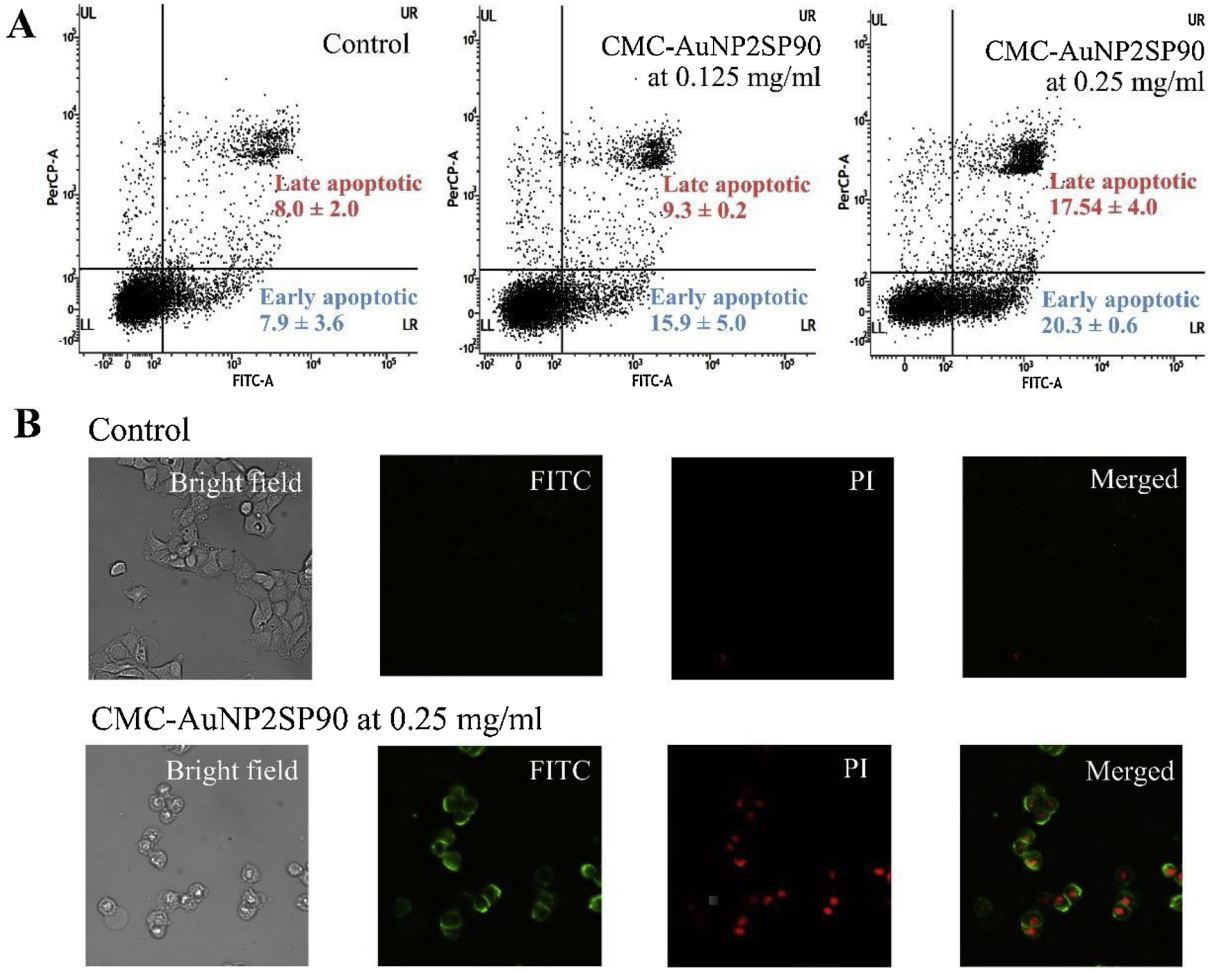

Fig. 7. (A) Dot plots of annexin V-PI staining apoptosis test of MCF-7 cells treated with CMC-AuNP2SP90 at concentrations of 0, 0.125 and 0.25 mg/mL for 24 h (n = 3). (B) Fluorescence images of MCF-7 cells treated with CMC-AuNP2SP90 for 24 h. (Note: Green and red colors represent the damaged membrane of the viable cells and leakage of cytoplasmic constituents of the death cells, respectively. Cells with green staining represent early apoptotic; cells with both green and red staining were scored as late apoptotic cells and necrotic cells.) (For interpretation of the references to colour in this figure legend, the reader is referred to the web version of this article).

against cancer and normal cells of CMC-AuNPs by reducing not only the D_H of CMC-AuNPs but also the size and size distribution of AuNPs existing in CMC-AuNPs. During the plasma discharge in an aqueous solution containing water, a variety of highly reactive species, such as $^{\cdot}$OH and $^{\cdot}$H, could be generated. The generated $^{\cdot}$OH usually plays an important role in the degradation of biopolymers (Chokradjaroen et al., 2018), including CMC; moreover, $^{\cdot}$OH can undergo the recombination reaction to produce H_2O_2, leading to the decreasing of pH of the solution. As prolonging the plasma discharge time, the pH of the solution gradually decreased, resulting in a smaller size of AuNPs due to the partial dissolution of AuNPs at acidic pH (Saito et al., 2009). Accordingly, the SP treatment could reduce the D_H of CMC-AuNPs by decreasing both the polymer chain length of CMC and the particle size of AuNPs. As a result, CMC-AuNPs having a suitable size, *i.e.* less than 100 nm, for cellular uptakes could be obtained. By this way, the SP-treated CMC-AuNPs could enhance cellular responses of cancer cells because of the relatively high metabolism rate of cancer cells compared with normal cells (Fadaka et al., 2017).

4. Conclusion

Since electrical discharge plasma in a liquid phase, so-called solution plasma (SP), can facilitate degradation of biopolymers without the addition of acids and oxidizing agents, SP is an interesting tool for applications in biomedical field. Furthermore, biological activities of some biopolymers may be enhanced when their molecular weights are low enough for a better cellular uptake. In this study, SP was used in preparation of colloidal gold nanoparticles (AuNPs) stabilized with *N,O*-carboxymethyl chitosan (CMC). Although AuNPs, CMC and CMC-stabilized AuNPs (CMC-AuNPs) exhibited low cytotoxicity against the breast cancer cell line (MCF-7), the SP-treated CMC-AuNPs could significantly reduce the cell viability of MCF-7. The evidences indicated that the plasma treatment could considerably reduce molecular weight of CMC, leading to the smaller hydrodynamic diameters of the SP-treated CMC-AuNPs. Moreover, the SP-treated CMC-AuNPs had much lower negative magnitudes of zeta potential than CMC and CMC-AuNPs while colloidal stability of the SP-treated CMC-AuNPs could be maintained. By this way, the cellular uptake of the SP-treated CMC-AuNPs was possibly increased, resulting in the higher cytotoxicity against MCF-7. However, further studies still require to examine the presence of the SP-treated CMC-AuNPs in living cells in order to find out the cause of cell death.

CRediT authorship contribution statement

Chayanaphat Chokradjaroen: Investigation, Writing - original draft. **Ratana Rujiravanit:** Funding acquisition, Supervision, Writing - review & editing. **Sewan Theeramunkong:** Investigation. **Nagahiro Saito:** Resources.

Acknowledgements

CC would like to thank Dr. Gasidit Panomsuwan for providing pure gold nanoparticles. This work was financially supported by the Thailand Research Fund (TRF) under the contract number BRG5480008 and JST/CREST under the grant number GJPMJCR12L1. The authors thank Surapon Foods Public Co., Ltd. (Thailand) for providing the shrimp shells and the NU-PPC Plasma Chemical Technology Laboratory at Chulalongkorn University (Thailand) and JSPS Core-to-Core Program, B. Asia-Africa Science Platforms for providing the financial support and equipments for experimental setup of solution plasma. All facilities for biological tests were supported by Drug Discovery and Development Center, Office of Advanced Science and Technology, Thammasat University (Thailand).

Appendix A. Supplementary data

Supplementary material related to this article can be found, in the online version, at doi:https://doi.org/10.1016/j.carbpol.2020.116162.

References

Albanese, A., & Chan, W. C. W. (2011). Effect of gold nanoparticle aggregation on cell uptake and toxicity. *ACS Nano, 5*.

Anitha, A., Maya, S., Deepa, N., Chennazhi, K. P., Nair, S. V., Tamura, H., et al. (2011). Efficient water soluble O-carboxymethyl chitosan nanocarrier for the delivery of curcumin to cancer cells. *Carbohydrate Polymers, 83*(2), 452–461.

Arvizo, R., Bhattacharya, R., & Mukherjee, P. (2010). Gold nanoparticles: Opportunities and challenges in nanomedicine. *Expert Opinion on Drug Delivery, 7*(6), 753–763.

Baroch, P., Anita, V., Saito, N., & Takai, O. (2008). Bipolar pulsed electrical discharge for decomposition of organic compounds in water. *Journal of Electrostatics, 66*(5–6), 294–299.

Bastús, N. G., Comenge, J., & Puntes, V. (2011). Kinetically controlled seeded growth synthesis of citrate-stabilized gold nanoparticles of up to 200 nm: Size focusing versus ostwald ripening. *Langmuir, 27*(17), 11098–11105.

Boisselier, E., & Astruc, D. (2009). Gold nanoparticles in nanomedicine: Preparations, imaging, diagnostics, therapies and toxicity. *Chemical Society Reviews, 38*(6), 1759–1782.

Boyles, M. S. P., Kristl, T., Andosch, A., Zimmermann, M., Tran, N., Casals, E., et al. (2015). Chitosan functionalisation of gold nanoparticles encourages particle uptake and induces cytotoxicity and pro-inflammatory conditions in phagocytic cells, as well as enhancing particle interactions with serum components. *Journal of Nanobiotechnology, 13*(1), 84.

Brown, S. D., Nativo, P., Smith, J.-A., Stirling, D., Edwards, P. R., Venugopal, B., et al. (2010). Gold nanoparticles for the improved anticancer drug delivery of the active component of oxaliplatin. *Journal of the American Chemical Society, 132*(13), 4678–4684.

Cai, W., Gao, T., Hong, H., & Sun, J. (2008). Applications of gold nanoparticles in cancer nanotechnology. *Nanotechnology, Science and Applications, 2008*(1), https://doi.org/10.2147/NSA.S3788.

Chen, S.-C., Wu, Y.-C., Mi, F.-L., Lin, Y.-H., Yu, L.-C., & Sung, H.-W. (2004). A novel pH-sensitive hydrogel composed of N,O-carboxymethyl chitosan and alginate cross-linked by genipin for protein drug delivery. *Journal of Controlled Release, 96*(2), 285–300.

Chen, W., Li, Y., Yang, S., Yue, L., Jiang, Q., & Xia, W. (2015). Synthesis and antioxidant properties of chitosan and carboxymethyl chitosan-stabilized selenium nanoparticles. *Carbohydrate Polymers, 132*, 574–581.

Choi, J.-Y., Park, C. H., & Lee, J. (2008). Effect of polymer molecular weight on nano-comminution of poorly soluble drug. *Drug Delivery, 15*(5), 347–353.

Choi, S., Jang, S., Park, J., Jeong, S., Park, J., Ock, K., et al. (2012). Cellular uptake and cytotoxicity of positively charged chitosan gold nanoparticles in human lung adenocarcinoma cells. *Journal of Nanoparticle Research, 14*.

Chokradjaroen, C., Rujiravanit, R., Watthanaphanit, A., Theeramunkong, S., Saito, N., Yamashita, K., et al. (2017). Enhanced degradation of chitosan by applying plasma treatment in combination with oxidizing agents for potential use as an anticancer agent. *Carbohydrate Polymers, 167*, 1–11.

Chokradjaroen, C., Theeramunkong, S., Yui, H., Saito, N., & Rujiravanit, R. (2018). Cytotoxicity against cancer cells of chitosan oligosaccharides prepared from chitosan powder degraded by electrical discharge plasma. *Carbohydrate Polymers, 201*, 20–30.

El-Brolossy, T. A., Abdallah, T., Mohamed, M. B., Abdallah, S., Easawi, K., Negm, S., et al. (2008). Shape and size dependence of the surface plasmon resonance of gold nanoparticles studied by Photoacoustic technique. *The European Physical Journal Special Topics, 153*(1), 361–364.

El-Sawy, N. M., Abd El-Rehim, H. A., Elbarbary, A. M., & Hegazy, E.-S. A. (2010). Radiation-induced degradation of chitosan for possible use as a growth promoter in agricultural purposes. *Carbohydrate Polymers, 79*(3), 555–562.

Erdemi, H., Baykal, A., Karaoğlu, E., & Toprak, M. S. (2012). Synthesis and conductivity studies of piperidine-4-carboxylic acid functionalized Fe3O4 nanoparticles. *Materials Research Bulletin, 47*(9), 2193–2199.

Fadaka, A., Ajiboye, B., Ojo, O., Adewale, O., Olayide, I., & Emuowhochere, R. (2017). Biology of glucose metabolization in cancer cells. *Journal of Oncological Sciences, 3*(2), 45–51.

Fenger, R., Fertitta, E., Kirmse, H., Thünemann, A. F., & Rademann, K. (2012). Size dependent catalysis with CTAB-stabilized gold nanoparticles. *Physical Chemistry Chemical Physics, 14*(26), 9343–9349.

Fernandes, J. C., Eaton, P., Nascimento, H., Gião, M. S., Ramos, Ó. S., Belo, L., et al. (2010). Antioxidant activity of chitooligosaccharides upon two biological systems: Erythrocytes and bacteriophages. *Carbohydrate Polymers, 79*(4), 1101–1106.

Fernández-Martín, F., Arancibia, M., López-Caballero, E., Gómez-Guillén, C., Montero, P., & Fernández-García, M. (2014). Preparation and molecular characterization of chitosans obtained from shrimp (Litopenaeus vannamei) shells. *Journal of Food Science, 79*(9), E1722–E1731.

Gibot, L., Chabaud, S., Bouhout, S., Bolduc, S., Auger, F. A., & Moulin, V. J. (2015). Anticancer properties of chitosan on human melanoma are cell line dependent. *International Journal of Biological Macromolecules, 72*, 370–379.

Gu, C., Sun, B., Wu, W., Wang, F., & Zhu, M. (2007). Synthesis, characterization of copper-loaded carboxymethyl-chitosan nanoparticles with effective antibacterial activity. *Macromolecular Symposia, 254*(1), 160–166.

Haesuwannakij, S., Kimura, T., Furutani, Y., Okumura, K., Kokubo, K., Sakata, T., et al. (2017). The impact of the polymer chain length on the catalytic activity of poly(N-vinyl-2-pyrrolidone)-supported gold nanoclusters. *Scientific Reports, 7*(1), 9579.

Han, F.-S., Cui, B.-H., You, X.-F., Xing, Y.-F., & Sun, X.-W. (2015). Anti-proliferation and radiosensitization effects of chitooligosaccharides on human lung cancer line HepG2. *Asian Pacific Journal of Tropical Medicine, 8*(9), 757–761.

Heller, W., & Pugh, T. L. (1960). "Steric" stabilization of colloidal solutions by adsorption of flexible macromolecules. *Journal of Polymer Science, 47*(149), 203–217.

Hu, Q., Chen, N., Feng, C., Hu, W., & Liu, H. (2016). Kinetic and isotherm studies of nitrate adsorption on granular Fe–Zr–chitosan complex and electrochemical reduction of nitrate from the spent regenerant solution. *RSC Advances, 6*(66), 61944–61954.

Huang, K., Ma, H., Liu, J., Huo, S., Kumar, A., Wei, T., et al. (2012). Size-dependent localization and penetration of ultrasmall gold nanoparticles in cancer cells, multicellular spheroids, and tumors in vivo. *ACS Nano, 6*(5), 4483–4493.

Huang, R., Mendis, E., Rajapakse, N., & Kim, S.-K. (2006). Strong electronic charge as an important factor for anticancer activity of chitooligosaccharides (COS). *Life Sciences, 78*(20), 2399–2408.

Jain, P. K., El-Sayed, I. H., & El-Sayed, M. A. (2007). Au nanoparticles target cancer. *Nano Today, 2*(1), 18–29.

Jazayeri, M. H., Amani, H., Pourfatollah, A. A., Pazoki-Toroudi, H., & Sedighimoghaddam, B. (2016). Various methods of gold nanoparticles (GNPs) conjugation to antibodies. *Sensing and Bio-Sensing Research, 9*, 17–22.

Jiang, M., Wang, K., Kennedy, J. F., Nie, J., Yu, Q., & Ma, G. (2010). Preparation and characterization of water-soluble chitosan derivative by Michael addition reaction. *International Journal of Biological Macromolecules, 47*(5), 696–699.

Kalliola, S., Repo, E., Srivastava, V., Heiskanen, J. P., Sirviö, J. A., Liimatainen, H., et al. (2017). The pH sensitive properties of carboxymethyl chitosan nanoparticles cross-linked with calcium ions. *Colloids and Surfaces B: Biointerfaces, 153*, 229–236.

Kang, F., Qu, X., Alvarez, P. J. J., & Zhu, D. (2017). Extracellular saccharide-mediated reduction of Au^{3+} to gold nanoparticles: New insights for heavy metals biomineralization on microbial surfaces. *Environmental Science & Technology, 51*(5), 2776–2785.

Kang, J., Li, O. L., & Saito, N. (2013). Synthesis of structure-controlled carbon nano spheres by solution plasma process. *Carbon, 60*, 292–298.

Kannan, P., Los, M., Los, J. M., & Niedziolka-Jonsson, J. (2014). T7 bacteriophage induced changes of gold nanoparticle morphology: Biopolymer capped gold nanoparticles as versatile probes for sensitive plasmonic biosensors. *Analyst, 139*(14), 3563–3571.

Karaoğlu, E., Baykal, A., Şenel, M., Sözeri, H., & Toprak, M. S. (2012). Synthesis and characterization of piperidine-4-carboxylic acid functionalized Fe3O4 nanoparticles as a magnetic catalyst for Knoevenagel reaction. *Materials Research Bulletin, 47*(9), 2480–2486.

Kim, S.-K. (2010). *Chitin, chitosan, oligosaccharides and their derivatives: Biological activities and applications*. CRC Press.

Kim, D., Jeong, Y. Y., & Jon, S. (2010). A drug-loaded aptamer−gold nanoparticle bioconjugate for combined CT imaging and therapy of prostate cancer. *ACS Nano, 4*(7), 3689–3696.

Laudenslager, M. J., Schiffman, J. D., & Schauer, C. L. (2008). Carboxymethyl chitosan as a matrix material for platinum, gold, and silver nanoparticles. *Biomacromolecules, 9*(10), 2682–2685.

Li, P.-C., Liao, G. M., Kumar, S. R., Shih, C.-M., Yang, C.-C., Wang, D.-M., et al. (2016). Fabrication and characterization of chitosan nanoparticle-incorporated quaternized poly(vinyl alcohol) composite membranes as solid electrolytes for direct methanol alkaline fuel cells. *Electrochimica Acta, 187*, 616–628.

Medrzycka, K. B. (1991). The effect of particle concentration on zeta potential in extremely dilute solutions. *Colloid and Polymer Science, 269*(1), 85–90.

Nguyen, H. H., Park, J., Kang, S., & Kim, M. (2015). Surface plasmon resonance: A versatile technique for biosensor applications. *Sensors (Basel, Switzerland), 15*(5), 10481–10510.

Nivethaa, E. A. K., Dhanavel, S., Narayanan, V., Vasu, C. A., & Stephen, A. (2015). An in vitro cytotoxicity study of 5-fluorouracil encapsulated chitosan/gold nanocomposites towards MCF-7 cells. *RSC Advances, 5*(2), 1024–1032.

Oh, E., Delehanty, J. B., Sapsford, K. E., Susumu, K., Goswami, R., Blanco-Canosa, J. B., et al. (2011). Cellular uptake and fate of PEGylated gold nanoparticles is dependent on both cell-penetration peptides and particle size. *ACS Nano, 5*(8), 6434–6448.

Pengyang, W., Xin, W., Liming, W., Xiaoyang, H., Wei, L., & Chunying, C. (2015).

Interaction of gold nanoparticles with proteins and cells. *Science and Technology of Advanced Materials, 16*(3), 034610.
Pornsunthorntawee, O., Katepetch, C., Vanichvattanadecha, C., Saito, N., & Rujiravanit, R. (2014). Depolymerization of chitosan–metal complexes via a solution plasma technique. *Carbohydrate Polymers, 102*(0), 504–512.
Potocký, Š., Saito, N., & Takai, O. (2009). Needle electrode erosion in water plasma discharge. *Thin Solid Films, 518*(3), 918–923.
Prasertsung, I., Damrongsakkul, S., & Saito, N. (2013). Degradation of β-chitosan by solution plasma process (SPP). *Polymer Degradation and Stability, 98*(10), 2089–2093.
Prasertsung, I., Damrongsakkul, S., Terashima, C., Saito, N., & Takai, O. (2012). Preparation of low molecular weight chitosan using solution plasma system. *Carbohydrate Polymers, 87*(4), 2745–2749.
Qiu, Y., Liu, Y., Wang, L., Xu, L., Bai, R., Ji, Y., et al. (2010). Surface chemistry and aspect ratio mediated cellular uptake of Au nanorods. *Biomaterials, 31*(30), 7606–7619.
Saito, N., Bratescu, M. A., & Hashimi, K. (2017). Solution plasma: A new reaction field for nanomaterials synthesis. *Japanese Journal of Applied Physics, 57*(1) 0102A0104.
Saito, N., Hieda, J., & Takai, O. (2009). Synthesis process of gold nanoparticles in solution plasma. *Thin Solid Films, 518*(3), 912–917.
Selim, M. E., & Hendi, A. A. (2012). Gold nanoparticles induce apoptosis in MCF-7 human breast cancer cells. *Asian Pacific Journal of Cancer Prevention, 13*(4), 1617–1620.
Serro, A. P., Gispert, M. P., Martins, M. C. L., Brogueira, P., Colaço, R., & Saramago, B. (2006). Adsorption of albumin on prosthetic materials: Implication for tribological behavior. *Journal of Biomedical Materials Research Part A, 78A*(3), 581–589.
Shi, X., Du, Y., Yang, J., Zhang, B., & Sun, L. (2006). Effect of degree of substitution and molecular weight of carboxymethyl chitosan nanoparticles on doxorubicin delivery. *Journal of Applied Polymer Science, 100*(6), 4689–4696.
Shukla, R., Bansal, V., Chaudhary, M., Basu, A., Bhonde, R. R., & Sastry, M. (2005). Biocompatibility of gold nanoparticles and their endocytotic fate inside the cellular compartment: A microscopic overview. *Langmuir, 21*(23), 10644–10654.
Silva, A. T. B., Coelho, A. G., Lopes, L. C. D. S., Martins, M. V. A., Crespilho, F. N., Merkoçi, A., et al. (2013). Nano-assembled supramolecular films from chitosan-stabilized gold nanoparticles and cobalt(II) phthalocyanine. *Journal of the Brazilian Chemical Society, 24*, 1237–1245.
Sonavane, G., Tomoda, K., & Makino, K. (2008). Biodistribution of colloidal gold nanoparticles after intravenous administration: Effect of particle size. *Colloids and Surfaces B: Biointerfaces, 66*(2), 274–280.
Takai, O. (2014). Fundamentals and applications of solution plasma. *Journal of Photopolymer Science and Technology, 27*(3), 379–384.
Tantra, R., Schulze, P., & Quincey, P. (2010). Effect of nanoparticle concentration on zeta-potential measurement results and reproducibility. *Particuology, 8*(3), 279–285.
Thi Lanh, L., Quang Khieu, D., Thai Hoa, T., Hai Phong, N., Thi Le Hien, H., & Quoc Hien, N. (2014). Synthesis of water soluble chitosan stabilized gold nanoparticles and determination of uric acid. *Advances in Natural Sciences Nanoscience and Nanotechnology, 5*(2), 025014.
Tréguer-Delapierre, M., Majimel, J., Mornet, S., Duguet, E., & Ravaine, S. (2008). Synthesis of non-spherical gold nanoparticles. *Gold Bulletin, 41*(2), 195–207.
Uldry, M., Ibberson, M., Hosokawa, M., & Thorens, B. (2002). GLUT2 is a high affinity glucosamine transporter. *FEBS Letters, 524*(1), 199–203.
Uznanski, P., Zakrzewska, J., Favier, F., Kazmierski, S., & Bryszewska, E. (2017). Synthesis and characterization of silver nanoparticles from (bis)alkylamine silver carboxylate precursors. *Journal of Nanoparticle Research, 19*(3), 121.
Wang, L., Liu, Y., Li, W., Jiang, X., Ji, Y., Wu, X., et al. (2011). Selective targeting of gold nanorods at the mitochondria of cancer cells: Implications for cancer therapy. *Nano Letters, 11*(2), 772–780.
Watthanaphanit, A., & Saito, N. (2013). Effect of polymer concentration on the depolymerization of sodium alginate by the solution plasma process. *Polymer Degradation and Stability, 98*(5), 1072–1080.
Watthanaphanit, A., Panomsuwan, G., & Saito, N. (2014). A novel one-step synthesis of gold nanoparticles in an alginate gel matrix by solution plasma sputtering. *RSC Advances, 4*(4), 1622–1629.
Xia, W., Liu, P., Zhang, J., & Chen, J. (2011). Biological activities of chitosan and chitooligosaccharides. *Food Hydrocolloids, 25*(2), 170–179.
Xu, A., Yao, M., Xu, G., Ying, J., Ma, W., Li, B., et al. (2012). A physical model for the size-dependent cellular uptake of nanoparticles modified with cationic surfactants. *International Journal of Nanomedicine, 7*, 3547–3554.